



**HAL**  
open science

## Crystalline functionalized endohedral C<sub>60</sub> metallofullerides

Ayano Nakagawa, Makiko Nishino, Hiroyuki Niwa, Katsuma Ishino, Zhiyong Wang, Haruka Omachi, Ko Furukawa, Takahisa Yamaguchi, Tatsuhisa Kato, Shunji Bandow, et al.

► **To cite this version:**

Ayano Nakagawa, Makiko Nishino, Hiroyuki Niwa, Katsuma Ishino, Zhiyong Wang, et al.. Crystalline functionalized endohedral C<sub>60</sub> metallofullerides. Nature Communications, 2018, 9 (1), pp.3073. 10.1038/s41467-018-05496-8 . hal-01860239

**HAL Id: hal-01860239**

**<https://hal.science/hal-01860239v1>**

Submitted on 21 May 2024

**HAL** is a multi-disciplinary open access archive for the deposit and dissemination of scientific research documents, whether they are published or not. The documents may come from teaching and research institutions in France or abroad, or from public or private research centers.

L'archive ouverte pluridisciplinaire **HAL**, est destinée au dépôt et à la diffusion de documents scientifiques de niveau recherche, publiés ou non, émanant des établissements d'enseignement et de recherche français ou étrangers, des laboratoires publics ou privés.





Distributed under a Creative Commons Attribution 4.0 International License

ARTICLE

DOI: 10.1038/s41467-018-05496-8

OPEN

# Crystalline functionalized endohedral C<sub>60</sub> metallofullerides

Ayano Nakagawa<sup>1</sup>, Makiko Nishino<sup>1</sup>, Hiroyuki Niwa<sup>1</sup>, Katsuma Ishino<sup>1</sup>, Zhiyong Wang<sup>1</sup>, Haruka Omachi <sup>1</sup>, Ko Furukawa<sup>2</sup>, Takahisa Yamaguchi<sup>3</sup>, Tatsuhisa Kato<sup>3</sup>, Shunji Bandow<sup>4</sup>, Jeremy Rio<sup>5</sup>, Chris Ewels <sup>5</sup>, Shinobu Aoyagi<sup>6</sup> & Hisanori Shinohara<sup>1</sup>

Endohedral metallofullerenes have been extensively studied since the first experimental observation of La@C<sub>60</sub> in a laser-vaporized supersonic beam in 1985. However, most of these studies have focused on metallofullerenes larger than C<sub>60</sub> such as (metal)@C<sub>82</sub>, and there are no reported purified C<sub>60</sub>-based monomeric metallofullerenes, except for [Li@C<sub>60</sub>]<sup>+</sup>(SbCl<sub>6</sub>)<sup>-</sup> salt. Pure (metal)@C<sub>60</sub> compounds have not been obtained because of their extremely high chemical reactivity. One route to their stabilization is through chemical functionalization. Here we report the isolation, structural determination and electromagnetic properties of functionalized crystalline C<sub>60</sub>-based metallofullerenes Gd@C<sub>60</sub>(CF<sub>3</sub>)<sub>5</sub> and La@C<sub>60</sub>(CF<sub>3</sub>)<sub>5</sub>. Synchrotron X-ray single-crystal diffraction reveals that La and Gd atoms are indeed encapsulated in the I<sub>h</sub>-C<sub>60</sub> fullerene. The HOMO-LUMO gaps of Gd@C<sub>60</sub> and La@C<sub>60</sub> are significantly widened by an order of magnitude with addition of CF<sub>3</sub> groups. Magnetic measurements show the presence of a weak antiferromagnetic coupling in Gd@C<sub>60</sub>(CF<sub>3</sub>)<sub>3</sub> crystals at low temperatures.

<sup>1</sup>Department of Chemistry and Institute for Advanced Research, Nagoya University, Nagoya 464-8602, Japan. <sup>2</sup>Center for Coordination of Research Facilities, Institute for Research Promotion, Niigata University, Niigata 950-2181, Japan. <sup>3</sup>Graduate School of Human and Environmental Sciences, Kyoto University, Sakyo-ku, Kyoto 606-8501, Japan. <sup>4</sup>Faculty of Science and Technology, Department of Applied Chemistry, Meijo University, Nagoya 468-8502, Japan. <sup>5</sup>Institut des Matériaux Jean Rouxel (IMN), Université de Nantes, CNRS UMR6502, BP32229, 44322 Nantes, France. <sup>6</sup>Department of Information and Basic Science, Nagoya City University, Nagoya 467-8501, Japan. Correspondence and requests for materials should be addressed to C.E. (email: [chris.ewels@cnsr-immn.fr](mailto:chris.ewels@cnsr-immn.fr)) or to H.S. (email: [noris@nagoya-u.jp](mailto:noris@nagoya-u.jp))

**C**<sub>60</sub> fullerene is the most abundant member of the so-called fullerene family<sup>1–4</sup>. However, monomeric C<sub>60</sub>-based endohedral metallofullerenes (i.e., fullerenes with metal atom(s) encapsulated), referred to hereafter as M@C<sub>60</sub>, have not been obtained in macroscopic and pure form to date. Most previous studies on metallofullerenes reported during the past 25 years have focused on higher fullerenes than C<sub>60</sub> such as C<sub>80</sub>, C<sub>82</sub>, and C<sub>84</sub><sup>2</sup>, even though the presence of M@C<sub>60</sub> has been confirmed by mass spectrometry of supersonic cluster beams in the gas phase<sup>3</sup> as well as laser-vaporized processed soot<sup>4</sup>. Theoretical calculations also suggested the stability and possible structure of M@C<sub>60</sub><sup>5–7</sup>. An exception is [Li@C<sub>60</sub>]<sup>+</sup>(SbCl<sub>6</sub>)<sup>–</sup> salt, which was produced by Li-ion bombardment with C<sub>60</sub> onto a target plate in vacuum<sup>8, 9</sup>. Neutral Li<sup>+</sup>@C<sub>60</sub><sup>–</sup> radicals have been obtained by the electrochemical reduction of cationic Li<sup>+</sup>@C<sub>60</sub>; however, Li@C<sub>60</sub> oligomerizes<sup>10</sup> and has a dimerized form in the crystal<sup>11</sup>.

The inability to extract and purify M@C<sub>60</sub> is due to their very small highest occupied molecular orbital-lowest unoccupied molecular orbital (HOMO-LUMO) gaps predicted, which lead to high chemical reactivity toward surrounding soot, air, moisture, and various organic solvents. There have been, however, several attempts<sup>12–15</sup> to try and extract and purify M@C<sub>60</sub> by, for example, vacuum sublimation from soot followed by liquid chromatographic separation<sup>13, 14</sup>. Unfortunately, none of these efforts led to the final macroscopic preparation of pure and isolated M@C<sub>60</sub>. For this reason, M@C<sub>60</sub> are often referred to as the missing metallofullerenes<sup>2, 16, 17</sup>.

One of the main reasons for the long-standing interest in M@C<sub>60</sub> is due to their expected novel electronic and magnetic behavior at low temperatures such as superconductivity, because the electronic band structures near the Fermi levels of M<sup>3+</sup>@C<sub>60</sub><sup>3–</sup> solids resemble those of superconducting alkali-doped C<sub>60</sub> fullerenes such as (K<sub>3</sub>)<sup>3+</sup>C<sub>60</sub><sup>3–</sup><sup>18</sup>. If this is the case, the presence of heavy atoms like lanthanoid elements inside C<sub>60</sub> might enhance the superconducting transition temperatures<sup>19</sup>. One way to stabilize such species and open the HOMO-LUMO gap is through chemical functionalization. Here we report the macroscopic preparation of purified (>99.9%) trifluoromethylated Gd@C<sub>60</sub> and La@C<sub>60</sub>, stable as Gd@C<sub>60</sub>(CF<sub>3</sub>)<sub>3,5</sub> and La@C<sub>60</sub>(CF<sub>3</sub>)<sub>3,5</sub>, respectively, and their structural determination, and electronic and magnetic properties.

## Results

**Enhanced stabilization of Gd@C<sub>60</sub> and La@C<sub>60</sub>.** To stabilize Gd@C<sub>60</sub> and La@C<sub>60</sub>, we have employed in situ trifluoromethylation during the arc-discharge synthesis of the metallofullerenes developed in the present laboratory (see Supplementary Discussion 1 and Supplementary Figure 1)<sup>11, 19</sup>. For example, the in situ trifluoromethylation of Gd@C<sub>60</sub> generates Gd@C<sub>60</sub>(CF<sub>3</sub>)<sub>*n*</sub> (*n* = 1–6) together with other sizes of trifluoromethylated Gd-metallofullerenes, Gd@C<sub>2*m*</sub>(CF<sub>3</sub>)<sub>*n*</sub> (2*m* ≥ 70) (see Supplementary Figures 2 and 3 for La). The high-temperature arc-discharge induces evaporation of polytetrafluoroethylene (PTFE) placed near the arc zone to produce CF<sub>3</sub> radicals<sup>11</sup>. We found trifluoromethyl-derivatized metallofullerenes, Gd@C<sub>60</sub>(CF<sub>3</sub>)<sub>*n*</sub> and La@C<sub>60</sub>(CF<sub>3</sub>)<sub>*n*</sub> (*n* = 3, 5), were formed efficiently. Trifluoromethyl derivatives of Gd@C<sub>60</sub> and La@C<sub>60</sub> are totally soluble and stable in toluene and carbon disulfide, which enabled us to perform high-performance liquid chromatography (HPLC) purification and thus subsequent characterization. As discussed in later sections, the stability of these trifluoromethyl derivatives, Gd@C<sub>60</sub>(CF<sub>3</sub>)<sub>3,5</sub> and La@C<sub>60</sub>(CF<sub>3</sub>)<sub>3,5</sub>, can be attributed to their closed-shell electronic structures, leading to wider HOMO-LUMO gaps than those of pristine Gd@C<sub>60</sub> and La@C<sub>60</sub>, respectively. With the current separation/

isolation protocol (see Supplementary Figure 4), one may, for example, obtain ca. 1.0–2.0 mg of purified (>99.9%) Gd@C<sub>60</sub>(CF<sub>3</sub>)<sub>5</sub> within 24 h from the initial *o*-xylene extraction of the soot containing Gd@C<sub>2*m*</sub>(CF<sub>3</sub>)<sub>*n*</sub> obtained by 10 arc-discharge syntheses (see Supplementary Figures 5–8). The absorption onsets of the ultraviolet-visible-near-infrared (UV-Vis-NIR) absorption spectra of CS<sub>2</sub> solution of Gd@C<sub>60</sub>(CF<sub>3</sub>)<sub>5</sub> and La@C<sub>60</sub>(CF<sub>3</sub>)<sub>5</sub> suggest the presence of enlarged HOMO-LUMO gaps of ca. 1.2 eV approaching that of C<sub>60</sub> (1.6 eV) (see Supplementary Figure 9). Interestingly, Gd@C<sub>60</sub>(CF<sub>3</sub>) and Gd@C<sub>60</sub>(CF<sub>3</sub>)<sub>2</sub> have not been solvent-extracted because of their much smaller HOMO-LUMO gaps even though mass spectrometric analysis indicates the presence of these metallofullerenes in raw soot.

Because of the very high reactivity of M@C<sub>60</sub>, it has not been self-evident that the metal is encapsulated in the conventional truncated icosahedral I<sub>h</sub>-C<sub>60</sub>. The C<sub>60</sub> might have a so-called non-isolated pentagon rule (non-IPR) structure<sup>20, 21</sup>, where two (or three) pentagons are fused with each other, since non-IPR fullerenes have frequently been observed in metallofullerenes during the past decade<sup>2</sup>. To answer this question, the molecular and crystal structures of Gd@C<sub>60</sub>(CF<sub>3</sub>)<sub>5</sub> (structural isomers I and II) and La@C<sub>60</sub>(CF<sub>3</sub>)<sub>5</sub> (I) have been determined by synchrotron radiation single-crystal X-ray diffraction (XRD) at SPring-8 (see Supplementary Tables 1–5).

**Synchrotron single-crystal XRD measurements.** The X-ray results clearly show that the C<sub>60</sub> cage structures of Gd@C<sub>60</sub>(CF<sub>3</sub>)<sub>5</sub> (I, II) and La@C<sub>60</sub>(CF<sub>3</sub>)<sub>5</sub> (I) are very similar to that of the conventional empty C<sub>60</sub>(I<sub>h</sub>). The five CF<sub>3</sub> groups of isomer I are attached to carbon atoms numbered as 6, 9, 12, 15, and 53 in a Schlegel diagram shown in Fig. 1a. In isomer II the five CF<sub>3</sub> groups are attached to carbon atoms numbered as 6, 9, 12, 15, and 36. In both isomers, four of the five CF<sub>3</sub> groups are attached to carbon atoms 6, 9, 12, and 15 bonded to carbon atoms 5, 1, 2, and 3 on a pentagon. Figure 1b–e shows the molecular structures of Gd@C<sub>60</sub>(CF<sub>3</sub>)<sub>5</sub>(I) and (II), respectively. Very interestingly, the remaining CF<sub>3</sub> group is attached not to carbon atom 18 but to carbon atom 53 (isomer I) or 36 (isomer II) located far from the 1-2-3-4-5 pentagon. This asymmetric attachment of five CF<sub>3</sub> groups results in C<sub>1</sub> symmetry. If the fifth CF<sub>3</sub> group had been attached to carbon atom 18, neighbouring carbon atom 4 on the pentagon, the molecule would have had five-fold symmetry. Instead of the fifth CF<sub>3</sub> group, a Gd (La) atom inside the C<sub>60</sub> cage is located near carbon atoms 18 and 4. The distances between the Gd atom and carbon atoms 18 and 4 are ~2.38 Å in both isomers (see Supplementary Tables 2–5).

The selective location of the Gd (La) atom is explained in terms of the elongation of C–C bond lengths by the attachment of CF<sub>3</sub> groups. The conventional C<sub>60</sub>(I<sub>h</sub>) molecule consists of two kinds of C–C bonds: short 6:6 bonds fusing two hexagons with a bond length of 1.39 Å and longer 6:5 bonds fusing a hexagon and a pentagon with a bond length of 1.45 Å. As expected, the C–C bonds around the carbon atoms with CF<sub>3</sub> groups attached (6, 9, 12, 15, and either 53 or 36) have *sp*<sup>3</sup> character, resulting in the elongation of the bonds. The 6:6 bond lengths between 6-5, 9-1, 12-2, and 15-3 carbon atoms are ~1.51 Å in both of the isomers (see Supplementary Tables 2 and 5). The 6:6 bond lengths between 18 and 4 atoms (~1.46 Å) are also longer than the normal 6:6 bond length (1.39 Å). This suggests that the Gd is interacting with the *p*<sub>z</sub>-orbitals of atoms 18 and 4, resulting in the breaking of the *π*-bond and elongation of the bond length. At the same time, there is a general attraction for the Gd toward the area of the C<sub>60</sub> surface that has been functionalized, hence this location beneath two carbon atoms rather than staying at the center of the neighboring hexagon.

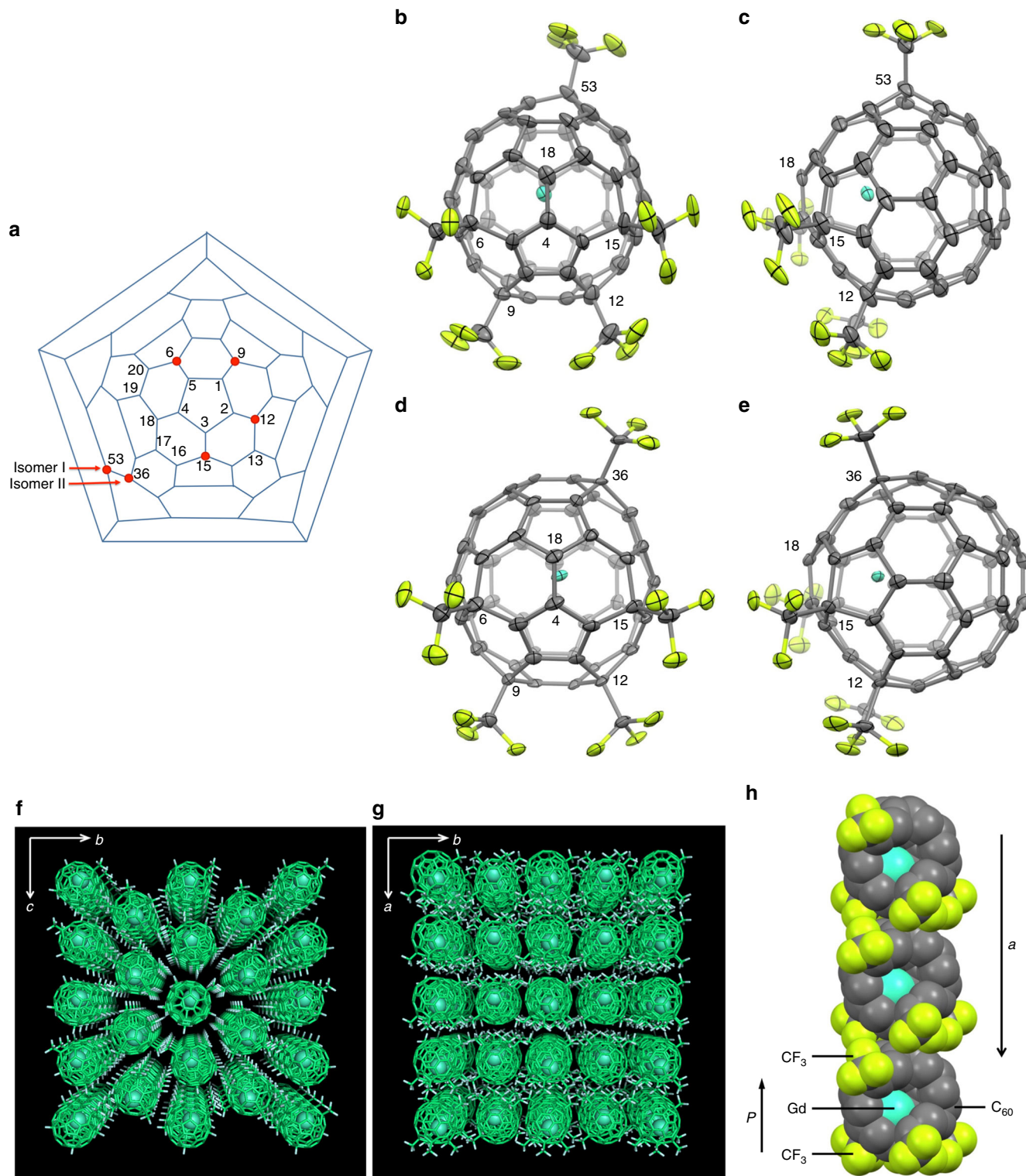


**Fig. 1**  $\text{Gd}@C_{60}(\text{CF}_3)_5$  (I) and (II). **a** Schlegel diagram of  $C_{60}$ .  $\text{CF}_3$  groups attached to  $\text{Gd}@C_{60}(\text{CF}_3)_5$  (I) and (II) are shown as red circles. **b, c** Molecular structure of  $\text{Gd}@C_{60}(\text{CF}_3)_5$  (I). **d, e** Molecular structure of  $\text{Gd}@C_{60}(\text{CF}_3)_5$  (II). Front views facing the bond between carbon atoms 4 and 18 (**b, d**) and side views (**c, e**) are shown. The thermal ellipsoids in (**b–e**) are drawn at 50% probability level. **f, g** Molecular packing in the  $\text{Gd}@C_{60}(\text{CF}_3)_5$  (I) crystal viewed along the  $a$ - and  $c$ -axis, respectively. Pseudo-hexagonal close-packed layers in the  $bc$ -plane are stacked along the  $a$ -axis. **h** Steric and electrostatic stacking of the  $\text{Gd}@C_{60}(\text{CF}_3)_5$  (I) molecules with an electric dipole moment ( $P$ ) along the  $a$ -axis, which form a close-packed array

$\text{Gd}@C_{60}(\text{CF}_3)_5$  (I) and  $\text{La}@C_{60}(\text{CF}_3)_5$  (I) form pure crystals that contain neither solvent nor ligand molecules. Figure 1f, g shows the molecular packing of the  $\text{Gd}@C_{60}(\text{CF}_3)_5$  (I) crystal. The centrosymmetric crystal with a space group of  $P2_1/c$  contains

two chiral isomers of  $\text{Gd}@C_{60}(\text{CF}_3)_5$  (I) with the same number of molecules. Most of the endohedral metallofullerene crystals so far reported contain either solvent or ligand molecules<sup>2</sup>.  $\text{Gd}@C_{60}(\text{CF}_3)_5$  (II) has been obtained only as a co-crystal with Ni



(OEP) (OEP: octaethylporphyrin). The crystals of  $\text{Gd@C}_{60}(\text{CF}_3)_5$  (I) and  $\text{La@C}_{60}(\text{CF}_3)_5$  (I) are the first example of pure crystals of  $\text{M@C}_{60}$  derivative. The crystal structure determined possesses a pseudo-hexagonal close-packed layer of the molecules in the  $bc$ -plane (Fig. 1f) and stacking of the layers along the  $a$ -axis (Fig. 1g). The stacking of the molecules is caused by inter-molecular steric and electrostatic interactions. The molecule has an electric dipole moment ( $P$ ) because of the electron-withdrawing  $\text{CF}_3$  groups asymmetrically attached to the  $\text{C}_{60}$  cage and the presence of the off-centered Gd (La) atom inside. The stacking of the turtle-like molecules with an electric dipole moment can provide an electrostatically stable close-packed array along the  $a$ -axis as shown in Fig. 1h (see Supplementary Figures 10–11). The detailed crystallographic data are summarized in Supplementary Tables 1–6.

We then carried out  $^{19}\text{F}$ -nuclear magnetic resonance (NMR) measurements of  $\text{La@C}_{60}(\text{CF}_3)_n$  (see Supplementary Discussion 3 and Supplementary Figure 14). The spectra of the two  $\text{La@C}_{60}(\text{CF}_3)_5$  isomers consist of five equal-intensity peaks, which are four quartets (or multiplets) due to the through-space coupling of the four grouped  $\text{CF}_3$  units and the other singlet due to fifth more isolated  $\text{CF}_3$  unit<sup>22, 23</sup>. In contrast, the  $^{19}\text{F}$ -NMR spectrum of  $\text{La@C}_{60}(\text{CF}_3)_3$  only showed a singlet peak at  $-75.5$  ppm because the three trifluoromethyl groups are geometrically equivalent, indicating  $\text{C}_3$  symmetry of  $\text{La@C}_{60}(\text{CF}_3)_3$ .

## Discussion

To obtain information on the growth mechanism, structure and electronic properties of  $\text{Gd@C}_{60}(\text{CF}_3)_5$ , we perform spin unrestricted density functional calculations under the local spin density approximation<sup>24–26</sup>, applying relativistic pseudopotentials<sup>27</sup>. Wavefunctions are constructed from 38/90/28 independent Gaussian-based functions for C/Gd/F, respectively, up to  $l = 3$  angular momentum, with an electron temperature of  $k_{\text{B}}T = 0.04$  eV for level occupation and 300 Ha cut-off plane-waves for the charge density. To explore the addition pathways for  $\text{CF}_3$  functionalization of  $\text{Gd@C}_{60}(\text{CF}_3)_n$ ,  $n = 0-5$ , we assume that  $\text{CF}_3$  adds to the most thermodynamically favored site and is then immobile, which is justified by a calculated high surface migration barrier of  $\text{CF}_3$  ( $n = 1$ ) of 59 kcal mol<sup>-1</sup>. Taking the most stable  $n$ th isomer as a starting point for  $n + 1$  stepwise addition allows us to reduce the number of isomers considered to a manageable several hundreds. Where two stable isomers are closer in energy than 2.3 kcal/mol of each other, we have used both as starting points for subsequent addition, allowing us to trace bifurcations in the addition pathway.

The Gd atom in  $\text{Gd@C}_{60}$  is initially covalently bound beneath hexagon (3-4-15-16-17-18) with 2.41 Å Gd–C bond lengths. The most stable  $\text{CF}_3$  addition pathway involves sequential addition to back bonds of the 1-2-3-4-5 pentagon, i.e., addition at sites 6, 9, 12, and 15 in that order shown in top line of Fig. 2a. Instead of completing the pentagon at site 18, which is excluded due to the presence of Gd below this last pentagon back bond with  $\sim 2.35$  Å Gd–C bond lengths, the fifth  $\text{CF}_3$  group adds behind the neighboring pentagon at sites 53 (isomer I) or 36 (isomer II). Adding a sixth  $\text{CF}_3$  group is endothermic compared to  $\frac{1}{2}(\text{CF}_3)_2$ , confirming that  $n = 5$  is the end point in the addition sequence in agreement with the experimental observation. Interestingly, isomer II matches a  $\text{La@C}_{60}(\text{CF}_3)_5$  structure proposed previously<sup>7</sup>, but the intermediate  $n = 4$  structure proposed there is different to the structure we find here and can only be linked to  $n = 3$  and 5 with additional surface  $\text{CF}_3$  migration.

After  $n = 1$  addition at site 6 there is a second stable isomer for  $n = 2$ , where Gd maintains its hexagonal site and  $\text{CF}_3$  adds to site 36 (lower line of Fig. 2a). The pathway then bifurcates once again, the energetically favored route continuing the 9, 12, 15 addition

sequence to isomer II. However, an alternative  $n = 3$  addition at site 13 results instead in a  $\text{C}_3$  symmetry  $\text{Gd@C}_{60}(\text{CF}_3)_3$  isomer. Further  $\text{CF}_3$  addition to this is endothermic, showing this to be a third stable end point in the addition sequence. This mapping process thus shows remarkable agreement with the current X-ray and  $^{19}\text{F}$ -NMR experimental results, successfully predicting the three observed  $\text{Gd@C}_{60}(\text{CF}_3)_n$  species, i.e.,  $\text{Gd@C}_{60}(\text{CF}_3)_5$  (I),  $\text{Gd@C}_{60}(\text{CF}_3)_5$  (II) and  $\text{Gd@C}_{60}(\text{CF}_3)_3$ .

These three stable isomers have multiplicity 7/2, associated with the Gd atom. They are closed-shell systems (unlike many of the less-stable isomers), restoring the gap between HOMO and LUMO to  $\sim 2/3$  that of  $\text{C}_{60}$  (Fig. 2b) with the largest gap for  $\text{Gd@C}_{60}(\text{CF}_3)_3$ . The unpaired Gd  $f$ -states are deep lying with the HOMO and LUMO localized primarily over the fullerene cage with minor  $\text{CF}_3$  character (Fig. 2c). Gd plays an interesting dual role when selecting  $\text{CF}_3$  addition sites, acting as donor and localizing surface charge, while also affecting surface chemistry through strong hybridization with the carbon  $2p$  states. This suggests different addition sequences are likely for non-covalently bound endohedral  $+3$  oxidation species. As seen above, the agreement between the X-ray and the theoretical results for the presence of the stable isomers of  $\text{Gd@C}_{60}(\text{CF}_3)_{3,5}$  strongly suggests that  $\text{CF}_3$  groups are sequentially added to  $\text{Gd@C}_{60}$  during the arc-discharge synthesis. The energy levels, HOMO-LUMO and spin-up and -down charge density for  $\text{Gd@C}_{60}(\text{CF}_3)_3$  and  $\text{Gd@C}_{60}(\text{CF}_3)_5$  (I,II) are shown in Supplementary Figures 15 and 16, respectively.

Literature calculations for  $\text{M@C}_{60}(\text{CF}_3)_3$  using comparable methods give a calculated HOMO-LUMO gap of 0.81 eV for  $\text{Y@C}_{60}(\text{CF}_3)_3$ <sup>16</sup>, and  $\sim 0.7$  eV for  $\text{La@C}_{60}(\text{CF}_3)_3$ <sup>7</sup>, at first sight in discrepancy with our significantly larger calculated gap for  $\text{Gd@C}_{60}(\text{CF}_3)_3$  of 1.4 eV. This is because the literature calculations consider a  $\text{M@C}_{60}(\text{CF}_3)_3$  isomer with the  $\text{CF}_3$  groups arranged around a shared pentagon. Our calculated HOMO-LUMO gap for this  $\text{Gd@C}_{60}(\text{CF}_3)_3$  isomer is indeed 0.78 eV, close to these values. However, we do not predict this structure to be stable in isolation but simply an intermediate structure en-route to the formation of isomer I and isomer II  $\text{Gd@C}_{60}(\text{CF}_3)_5$  structures. The  $\text{Gd@C}_{60}(\text{CF}_3)_3$  isomer we predict to be a stable end point is instead the  $\text{C}_3$  symmetry isomer shown in Fig. 2, with  $\text{CF}_3$  groups arranged symmetrically around a central hexagon. This arrangement of  $\text{CF}_3$  groups gives the much wider calculated HOMO-LUMO gap of 1.4 eV.

The magnetic properties of  $\text{Gd@C}_{60}(\text{CF}_3)_3$  metallofullerene was investigated by SQUID measurements (see Supplementary Discussion 5). The HOMO-LUMO gap of  $\text{Gd@C}_{60}(\text{CF}_3)_3$  (1.4 eV) is larger than that of  $\text{Gd@C}_{60}(\text{CF}_3)_5$  (1.2 eV) suitable for solvent extraction and HPLC isolation. Magnetization curves of solid  $\text{Gd@C}_{60}(\text{CF}_3)_3$  indicate no hysteresis as shown in Fig. 3, where the ordinate is normalized by experimentally determined saturation magnetization  $M_s$  of 41 108 emu · G mol<sup>-1</sup>. Except for the magnetization curve at 2 K, other data points are on the same curvature trace. When magnetic moments thermally fluctuate without strong interaction between the magnetic moments, magnetization curves are fitted by the following Brillouin function  $B_J(x)$

$$M = M_s B_J(x) \quad (1)$$

$$M_s = NgJ\mu_B \quad (2)$$

$$B_J(x) = \frac{2J+1}{2J} \coth\left(\frac{2J+1}{2J}x\right) - \frac{1}{2J} \coth\left(\frac{1}{2J}x\right) \quad (3)$$

$$x = \frac{gJ\mu_B H}{k_{\text{B}}T} \quad (4)$$

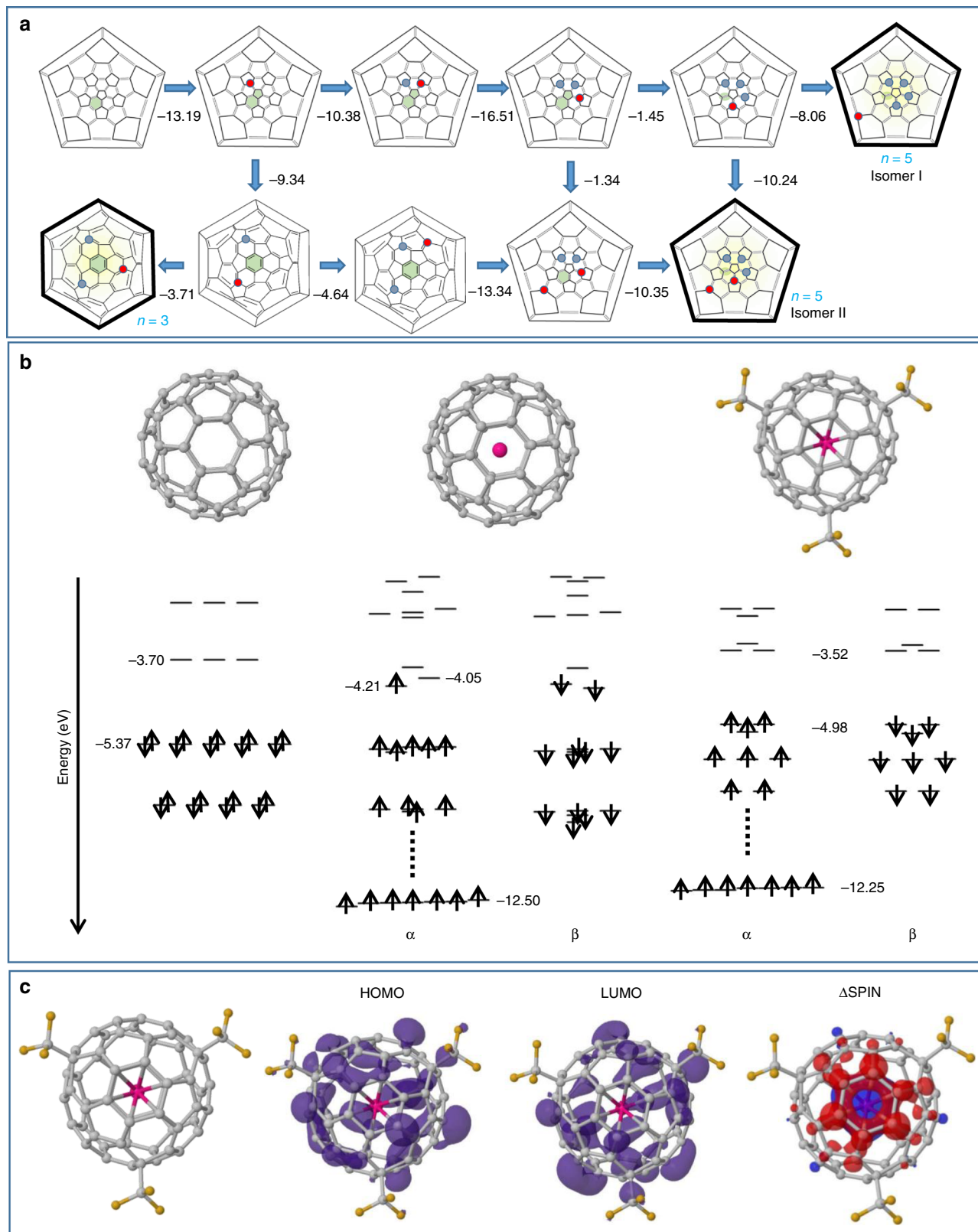


**Fig. 2** Calculated functionalization sequences and electronic properties of  $\text{Gd}@C_{60}(\text{CF}_3)_n$ . **a** Calculated preferential addition sequences for  $\text{CF}_3$  to  $\text{Gd}@C_{60}$ . Previous addition sites marked in blue, new addition site in red. Pink shading indicates location of the encapsulated Gd atom. Numbers indicate energy release in  $\text{kcal mol}^{-1}$  according to the reaction  $\text{Gd}@C_{60}(\text{CF}_3)_{n-1} + \frac{1}{2} (\text{CF}_3)_2 \rightarrow \text{Gd}@C_{60}(\text{CF}_3)_n$ . All pathways are shown where isomers are within  $2.3 \text{ kcal mol}^{-1}$  of the most stable. Fullerenes where next addition is endothermic have black outlines and represent stable end points of a reaction pathway.

**b** Calculated Kohn-Sham eigenvalues (eV) for (left)  $C_{60}$ , (center)  $\text{Gd}@C_{60}$ , and (right)  $\text{Gd}@C_{60}(\text{CF}_3)_3$ , showing  $\text{CF}_3$  functionalization results in a closed-shell system, reopening the HOMO-LUMO gap to nearly that of  $C_{60}$ . **c** Spatial distribution of calculated Kohn-Sham eigenstates showing highest occupied molecular orbital (HOMO) and lowest unoccupied molecular orbital (LUMO) and their neighboring states around the Fermi level for the most stable  $\text{Gd}@C_{60}(\text{CF}_3)_3(\text{I})$  isomer. The states are delocalized across the fullerene cage with very limited  $\text{CF}_3$  character

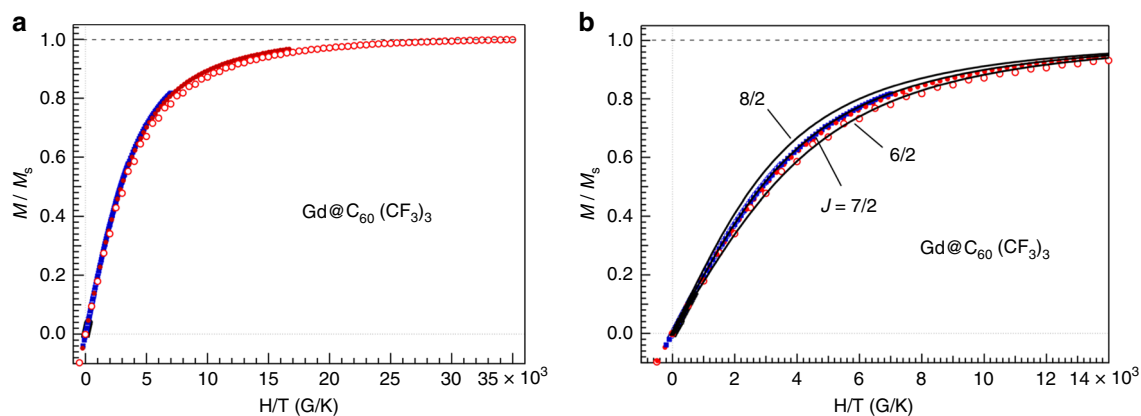


**Fig. 3** Normalized magnetization curves of  $\text{Gd@C}_{60}(\text{CF}_3)_3$ . **a** Whole trace of magnetization taken at 273, 100, 20, 10, 4.2, and 2 K, and **b** is an expansion around the origin of abscissa.  $M_s$  value determined experimentally is  $41108 \text{ emu} \cdot \text{G mol}^{-1}$ . Solid lines are the calculated magnetization curves using Brillouin function with  $J = 8/2, 7/2$ , and  $6/2$ . Red open circles are for the data taken at 2 K. Only this data set did not fit with the same curvature

where  $N$  is the spin concentration,  $g$  the  $g$ -factor,  $J$  the total quantum number,  $\mu_B$  the Bohr magneton, and  $k_B$  the Boltzmann constant. From the curve fitting, we found that the total quantum number  $J = 7/2$  is needed to explain the experimental results by setting  $g = 2$ . This gives an effective magnetic moment  $\mu_{\text{eff}} (= g\sqrt{J(J+1)}\mu_B)$  of  $7.94 \mu_B$  per  $\text{Gd@C}_{60}(\text{CF}_3)_3$  molecule. This experimental analysis supports a trivalent  $\text{Gd}^{3+}$  state by transferring three electrons to the  $\text{C}_{60}$  cage ( $\text{Gd}^{3+}@\text{C}_{60}^{3-}$ ) and these electrons are then used to make chemical bonds with three  $\text{CF}_3$  on  $\text{C}_{60}$ . Mulliken charge analysis shows that most of the transferred charge is indeed spread around the  $\text{C}_{60}$  cage beneath the  $\text{CF}_3$  groups, on the central pentagon, and on the neighbors of the Gd. The magnetic moment is thus essentially located on the encaged  $\text{Gd}^{3+}$  ion ( $4f^7, J = 7/2$  with orbital quantum number  $L = 0$ , i.e.,  $\text{Gd}^{3+}$  has spin  $7 \mu_B$ ) in agreement with the theoretical result shown in Fig. 2b. According to the previous studies on  $\text{M}^{3+}@\text{C}_{82}^{3-}$  ( $M = \text{Gd, Dy, Ho, Er}$ ) metallofullerenes<sup>28–32</sup>, the magnetic moments observed are significantly small compared to the expected moments of free  $\text{M}^{3+}$  ions.

This reduction of the magnetic moments was theoretically explained by antiferromagnetic coupling between the trivalent endohedral metals and free spins on the carbon cage<sup>33</sup>. In the present Gd (La)-encapsulating  $\text{C}_{60}$  fullerenes, since free spins on  $\text{C}_{60}$  are very small by forming the chemical bonds with  $\text{CF}_3$  on the cage, this guarantees an almost ideal magnetic moment of  $\text{Gd}^{3+}$  ion. Theoretically, a trace counter-spin can be seen localized on the  $\text{C}_{60}$  cage between the Gd and  $\text{CF}_3$  groups at 0 K (Fig. 2c), presumably too weak to be detectable by SQUID but partially responsible for the weak antiferromagnetic coupling observed at low temperature. This was also confirmed by the analysis of temperature dependence of molar magnetic susceptibility as explained in Supplementary Discussion 5.

To further investigate the electronic structures of  $\text{Gd@C}_{60}(\text{CF}_3)_5$  (I,II), we also performed electron spin resonance (ESR) measurements in  $\text{CS}_2$  frozen solution (see Supplementary Discussion 6 and Supplementary Table 7). The spectra recorded by an X-band continuous wave ESR spectrometer at 4 K and by a W-band at 20 K are shown in the upper and lower panels of Fig. 4, respectively, where the observed spectra with fine structure in red are compared with simulated ones in blue<sup>34, 35</sup>. The parameters shown in Supplementary Table 7 were determined so that both of the observed spectra by the X- and W-band measurements should simultaneously be reproduced by the simulation. In both cases the spin quantum number of  $S = 7/2$  was obtained, consistent with the theoretical and magnetic

measurement results described above. The zero-field splitting parameters,  $D = 0.162 \text{ cm}^{-1}$  and  $D = 0.193 \text{ cm}^{-1}$ , were obtained for  $\text{Gd@C}_{60}(\text{CF}_3)_5$  (I) and  $\text{Gd@C}_{60}(\text{CF}_3)_5$  (II), respectively, comparable to those for  $S = 7/2$  states of  $\text{Gd@C}_{82}$ <sup>34</sup> and  $\text{Eu@C}_{82}$ <sup>35</sup>. The lift of the  $x$  and  $y$  degeneracy of  $E = 0.012 \text{ cm}^{-1}$  for  $\text{Gd@C}_{60}(\text{CF}_3)_5$  (II), which is bigger than that ( $E = 0.000 \text{ cm}^{-1}$ ) of  $\text{Gd@C}_{60}(\text{CF}_3)_5$  (I), suggests that the position of the  $\text{Gd}^{3+}$  ions in the two isomers differs slightly, since the  $E$  parameters originate basically in the spin-orbit coupling of the  $\text{Gd}^{3+}$  ions. Our calculations indeed indicate that the  $\text{Gd}^{3+}$  ion of isomer (I) lies more symmetrically beneath the C–C bond (so more symmetrically with respect to the four  $\text{CF}_3$  groups around the pentagon) than that of isomer (II). The observed ESR parameters are summarized in Supplementary Table 7.

In summary, the missing metallofullerenes,  $\text{Gd@C}_{60}$  and  $\text{La@C}_{60}$ , in the trifluoromethylated forms of  $\text{Gd@C}_{60}(\text{CF}_3)_{3,5}$  and  $\text{La@C}_{60}(\text{CF}_3)_5$ , have been obtained in pure bulk forms. In situ trifluoromethylation widens the HOMO-LUMO gaps of  $\text{Gd@C}_{60}$  and  $\text{La@C}_{60}$ , enabling isolation of the metallofullerenes and the subsequent single-crystal synchrotron XRD. The crystals exhibit a pseudo-hexagonal close-packed layer of molecules in the  $bc$ -plane and stacking of the layers along the  $a$ -axis (a turtle-like stacked structure). The temperature dependence of the magnetic susceptibility of  $\text{Gd@C}_{60}(\text{CF}_3)_3$  is well fitted by the Curie-Weiss law. The magnetic moment is located on the encaged  $\text{Gd}^{3+}$  ion ( $4f^7, J = 7/2$  with orbital quantum number  $L = 0$ ), with very small magnetic moment on the cage in agreement with the theoretical results. The intact forms of  $\text{Gd@C}_{60}$  and  $\text{La@C}_{60}$  might exhibit superconductivity as the electronic structures resemble those of superconducting alkali-doped  $\text{C}_{60}$  fullerenes. The preparation and isolation of intact  $\text{Gd@C}_{60}$  fullerene is now underway in the present laboratory.

## Methods

**Synthesis, purification, and crystallization.** A cross-sectional view of the DC arc-discharge chamber is illustrated in Supplementary Figure 1, where PTFE rods (40 g) are placed near the discharge area. Graphite rods (100 g) impregnated with Gd (La) (0.8 mol%, Toyo Tanso Co.LTD) was used as the anode. A pure graphite rod (Toyo Tanso Co.LTD) was used as the cathode. Arc-discharge was performed at a DC current of 500 A in a flowing He atmosphere with a pressure of 7–9 kPa. During arc-discharge because of the high-temperature around the arc zone, PTFE was decomposed and evaporated to produce  $\text{CF}_3$  radicals. Normally, 50–70 g of raw soot was obtained per discharge. Gd-metallofullerenes and empty fullerenes were extracted from the raw soot with *o*-xylene.

**Extraction and separation.** The rapid separation of the metallofullerenes from empty fullerenes was carried out by the  $\text{TiCl}_4$  Lewis acid method developed in the



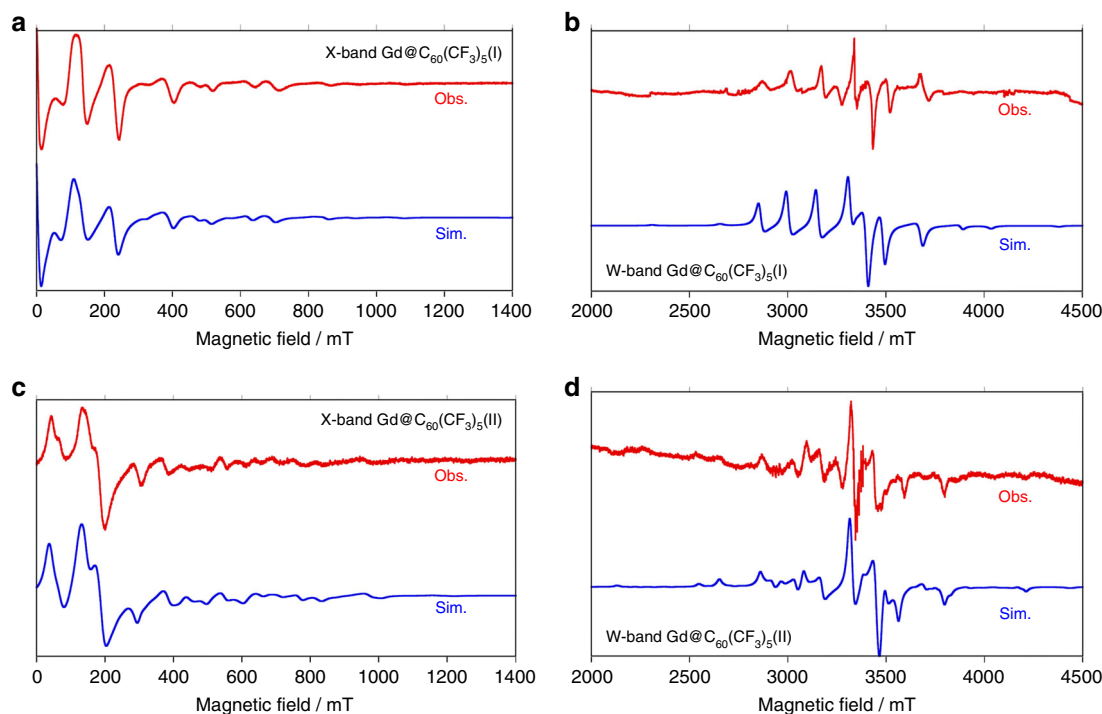


**Fig. 4** Confirmation of ESR parameters for  $\text{Gd@C}_{60}(\text{CF}_3)_5(\text{I})$  and  $\text{Gd@C}_{60}(\text{CF}_3)_5(\text{II})$ . **a, c** ESR spectra (red lines) of  $\text{Gd@C}_{60}(\text{CF}_3)_5(\text{I})$  and  $\text{Gd@C}_{60}(\text{CF}_3)_5(\text{II})$  recorded by X-band (9 GHz) spectrometer in  $\text{CS}_2$  at 4 K, **b, d** W-band (90 GHz) spectrometer in  $\text{CS}_2$  at 20 K. ESR parameters were determined so that both observed spectra in **a-d** should be simultaneously reproduced by simulation (blue lines)

present laboratory. To a 500 mL  $\text{CS}_2$  solution of the crude mixture of Gd-fullerenes and empty fullerenes, ca. 5 mL of  $\text{TiCl}_4$  was added. Metallofullerenes were reacted immediately and insoluble complexes were precipitated out. After mixing for 5 min, the precipitate was collected on a PTFE membrane filter and washed with 10–20 mL of  $\text{CS}_2$  to separate from the empty fullerenes solution. Deionized water was passed through the filter to decompose the complex of metallofullerene/ $\text{TiCl}_4$ , and then washed with acetone to eliminate extra water. Finally,  $\text{CS}_2$  was passed through the filter to collect desired Gd-metallofullerenes as a solution as shown in Supplementary Figure 2 (equivalent for La in Supplementary Figure 3).

**Multi-stage HPLC purification.** HPLC purification was conducted by using a JAI (Japan Analytical Industry Co. LTD.) recycling preparative HPLC LC-9104HS. The overall separation and isolation scheme of  $\text{Gd@C}_{60}(\text{CF}_3)_n$  is shown in Supplementary Figure 4. For the identification of metallofullerenes, mass spectrometric analysis was performed on Shimadzu MALDI-TOF-MS Spectrometer. Vis/NIR absorption spectra of metallofullerenes in  $\text{CS}_2$  were recorded by a Jasco V-570 spectrophotometer. Three isomers of  $\text{Gd@C}_{60}(\text{CF}_3)_n$  were isolated from the mixture by the multi-stage HPLC method developed in the present laboratory. Two kinds of columns were used alternatively with toluene eluent for the isolation, i.e., Buckyprep column (20 mm diameter  $\times$  250 mm, Nacalai Tesque Inc.) and Buckyprep-M column (20 mm diameter  $\times$  250 mm, Nacalai Tesque Inc.). The initial (the first stage) HPLC purification was performed with Buckyprep-M.  $\text{Gd@C}_{60}(\text{CF}_3)_n$  ( $n = 3, 5$ ) was obtained in fraction 1. The HPLC chromatograms are shown in Supplementary Figure 5 (equivalent for La in Supplementary Figure 6). Identification and isolation of the metallofullerenes were checked by MALDI mass spectroscopy as shown in Supplementary Figures 7 and 8. UV-Vis-NIR absorption spectra of the metallofullerenes exhibit characteristic features and also provide an estimate on their HOMO-LUMO gaps judging from the absorption onsets. The spectral features between Gd- and La-metallofullerenes are almost the same with each isomer as shown in Supplementary Figure 9.

**Synchrotron single-crystal X-ray structure analysis.** Single-crystal XRD measurements of  $\text{Gd@C}_{60}(\text{CF}_3)_5(\text{I})$ ,  $\text{La@C}_{60}(\text{CF}_3)_5(\text{I})$ ,  $\text{Gd@C}_{60}(\text{CF}_3)_5(\text{II})$ , and  $\text{Gd@C}_{60}(\text{CF}_3)_3$  were performed at SPring-8 BL02B1. The crystallographic data and various bond lengths for  $\text{Gd@C}_{60}(\text{CF}_3)_5(\text{I,II})$ ,  $\text{Gd@C}_{60}(\text{CF}_3)_3$ , and  $\text{La@C}_{60}(\text{CF}_3)_5(\text{I})$  are summarized in Supplementary Tables 1–6. The crystal structures for  $\text{Gd@C}_{60}(\text{CF}_3)_5(\text{I})$ ,  $\text{La@C}_{60}(\text{CF}_3)_5(\text{I})$ , and  $\text{Gd@C}_{60}(\text{CF}_3)_5(\text{II})$  are shown in Supplementary Figures 10–12, respectively. The charge density surface of  $\text{Gd@C}_{60}(\text{CF}_3)_3$  is shown in Supplementary Figure 13.

$\text{Gd@C}_{60}(\text{CF}_3)_5(\text{I})$  and  $\text{La@C}_{60}(\text{CF}_3)_5(\text{I})$ : Single crystals of  $\text{Gd@C}_{60}(\text{CF}_3)_5(\text{I})$  and  $\text{La@C}_{60}(\text{CF}_3)_5(\text{I})$  were obtained from  $\text{CS}_2$  solution by vapor diffusion.

Results of the XRD measurement are summarized in Supplementary Table 1.

The crystal structures were determined by using *SIR* and *SHELX* with good reliable factors.  $\text{Gd@C}_{60}(\text{CF}_3)_5(\text{I})$  and  $\text{La@C}_{60}(\text{CF}_3)_5(\text{I})$  have similar crystal structures. The centrosymmetric monoclinic crystals consist of the same number of two chiral isomers of the molecule. The unit cell contains two right-handed isomers and two left-handed isomers as shown in Supplementary Figures 10a and 11a. An independent molecule in the asymmetric unit has a disordered structure in which two chiral isomers overlap with the ratios of 0.8 and 0.2 as shown in Supplementary Figures 10b and 11b. In all, 95 C–C, 15 C–F, and 4 C–Gd (La) bond lengths of the major part of the disordered  $\text{Gd@C}_{60}(\text{CF}_3)_5(\text{I})$  and  $\text{La@C}_{60}(\text{CF}_3)_5(\text{I})$  are listed in Supplementary Tables 2 and 3, respectively. A total of 30 short 6:6 bonds fusing two hexagons and 60 long 6:5 bonds fusing a hexagon and a pentagon on the  $\text{C}_{60}$  cage are separately shown. The CIF deposition numbers at the Cambridge Crystallographic Data Centre (CCDC) are 1587428 for  $\text{Gd@C}_{60}(\text{CF}_3)_5(\text{I})$  and 1587430 for  $\text{La@C}_{60}(\text{CF}_3)_5(\text{I})$ .

$\text{Gd@C}_{60}(\text{CF}_3)_5(\text{II})$ : Single crystals of  $\text{Gd@C}_{60}(\text{CF}_3)_5(\text{II})$  were obtained from  $\text{CS}_2$  solution as co-crystals with Ni(OEP) by vapor diffusion. Results of the XRD measurement are summarized in Supplementary Table 4. The crystal structure was determined by using *SIR* and *SHELX* with a good reliable factor. The centrosymmetric triclinic crystals consist of the same number of two chiral isomers of  $\text{Gd@C}_{60}(\text{CF}_3)_5(\text{II})$ . The unit cell contains a right-handed isomer, a left-handed isomer, three Ni(OEP), and half toluene molecules as shown in Supplementary Figure 12a. An independent molecule in the asymmetric unit has a disordered structure in which two chiral isomers overlap with the ratios of 0.8 and 0.2 as shown in Supplementary Figure 12b. In all, 95 C–C, 15 C–F, and 4 C–Gd bond lengths of the major part of the disordered  $\text{Gd@C}_{60}(\text{CF}_3)_5(\text{II})$  are listed in Supplementary Table 5. A total of 30 short 6:6 bonds fusing two hexagons and 60 long 6:5 bonds fusing a hexagon and a pentagon on the  $\text{C}_{60}$  cage are separately shown. The CIF deposition number at CCDC is 1587429.

$\text{Gd@C}_{60}(\text{CF}_3)_3$ : Single crystals of  $\text{Gd@C}_{60}(\text{CF}_3)_3$  were obtained from  $\text{CS}_2$  solution by vapor diffusion. Results of the XRD measurement were summarized in Supplementary Table 6. The tetragonal unit cell can contain 16  $\text{Gd@C}_{60}(\text{CF}_3)_3$  molecules. An expected molecular arrangement was obtained by charge flipping using *Superflip* and maximum entropy method using *ENIGMA* as shown in Supplementary Figure 13. The figure shows an electron charge density surface obtained by maximum entropy method. A structure model with 16 double uniform shells of  $\text{Gd@C}_{60}$  located at  $(1/4 \pm 1/8, 1/4 \pm 1/8, 0)$ ,  $(-1/4 \pm 1/8, -1/4 \pm 1/8, 0)$ ,  $(1/4 \pm 1/8, -1/4 \pm 1/8, 1/2)$ , and  $(-1/4 \pm 1/8, 1/4 \pm 1/8, 1/2)$  was used in the analysis. Detailed structure of  $\text{Gd@C}_{60}(\text{CF}_3)_3$  could not be determined due to a severe orientation disorder and lack of resolution. We also attempted to obtain co-crystals of  $\text{Gd@C}_{60}(\text{CF}_3)_3$  with Ni(OEP); however, that have not been obtained.



**19F-NMR measurements.** NMR spectra were recorded on a JEOL ECS-400 spectrometer; chemical shifts for  $^{19}\text{F}$ -NMR (376 MHz,  $\text{CDCl}_3/\text{CS}_2$ ) are expressed in parts per million (ppm) relative to  $\text{C}_6\text{F}_6$  ( $\delta = -164.9$  ppm). Data are reported as follows: chemical shift; multiplicity (s = singlet, q = quartet, m = multiplet); coupling constant (Hz); and integration.  $\text{La}@C_{60}(\text{CF}_3)_3$ :  $\delta -75.5$  (s, 9F).  $\text{La}@C_{60}(\text{CF}_3)_5$  (I):  $\delta -79.4$  (s, 3F),  $-76.0$  (q,  $J = 10$  Hz, 3F),  $-74.9$  (q,  $J = 12$  Hz, 3F),  $-67.4$  (m, 3F), and  $-66.9$  (m, 3F).  $\text{La}@C_{60}(\text{CF}_3)_5$  (II):  $\delta -78.9$  (s, 3F),  $-78.0$  (q,  $J = 12$  Hz, 3F),  $-73.6$  (q,  $J = 10$  Hz, 3F),  $-68.3$  (m, 3F), and  $-67.3$  (m, 3F).

**SQUID magnetic measurement.** Sample dissolved in  $\text{CS}_2$  was transferred into quartz tube and the solution was vaporized under argon flow. Then the sample in quartz tube was evacuated by using turbo molecular pump at  $260^\circ\text{C}$  for 12 h and vacuum sealed. By this heat treatment, weight of  $\text{Gd}@C_{60}(\text{CF}_3)_3$  sample was decreased by ~65% (finally 0.71 mg of sample was loaded in the quartz tube), while no such weight change was observed for  $\text{La}@C_{60}(\text{CF}_3)_5$  one. Former finding suggests that the  $\text{CS}_2$  molecules were incorporated in a  $\text{Gd}@C_{60}(\text{CF}_3)_3$  solid, forming  $\text{Gd}@C_{60}(\text{CF}_3)_3(\text{CS}_2)_{6,4}$  just after vaporizing  $\text{CS}_2$  in Ar flow, and such incorporated  $\text{CS}_2$  molecules have been completely removed by heating at  $260^\circ\text{C}$  in vacuo. On the other hand, from the latter fact,  $\text{La}@C_{60}(\text{CF}_3)_5$  solid did not incorporate any  $\text{CS}_2$  molecule. That is, all SQUID measurements were carried out by using solution free samples. As described in the Discussion, magnetic behavior can be explained as an intramolecular feature and the interaction between the molecules is very small. Therefore, even if the sample incorporates some  $\text{CS}_2$  molecules, these molecules do not affect the present results.

**ESR measurements.** The X- and W-band ESR measurements were performed using a Bruker E500 and a E680 spectrometer, respectively. The temperature was controlled by helium flow cryostat (Oxford Instruments model ITC500). The X-band ESR spectra were measured at 4.0 K, and W-band ESR spectra were measured at 20 K. The spectral simulation were performed by using MATLAB software package with EasySpin toolbox. The observed ESR parameters are shown in Supplementary Table 7.

**Data availability.** Structural data are available in Supplementary Information. All additional data such as calculated xyz structures are available from the authors on request. The X-ray crystallographic coordinates for structures reported in this study have been deposited at the CCDC, under deposition numbers 1587428–1587430. These data can be obtained free of charge from The CCDC via [www.ccdc.cam.ac.uk/data\\_request/cif](http://www.ccdc.cam.ac.uk/data_request/cif).

Received: 22 January 2018 Accepted: 2 July 2018

Published online: 06 August 2018

## References

- Shinohara, H. Endohedral metallofullerenes. *Rep. Prog. Phys.* **63**, 843–892 (2000).
- Shinohara, H. & Tagmatarchis, N. *Endohedral Metallofullerenes—Fullerenes with Metal Inside* (Wiley, Chichester, 2015).
- Heath, J. R. et al. Lanthanum complexes of spheroidal carbon shells. *J. Am. Chem. Soc.* **107**, 7779–7780 (1985).
- Chai, Y. et al. Fullerenes with metals inside. *J. Phys. Chem.* **95**, 7564–7568 (1991).
- Rosen, A. & Waestberg, B. First-principle calculations of the ionization potentials and electron affinities of the spheroidal molecules  $\text{C}_{60}$  and  $\text{La}@C_{60}$ . *J. Am. Chem. Soc.* **110**, 8701–8703 (1988).
- Wang, L. S. et al. The electronic structure of  $\text{Ca}@C_{60}$ . *Chem. Phys. Lett.* **207**, 354–359 (1993).
- Guan, J. & Tomanek, D. Can  $\text{CF}_3$ -functionalized  $\text{La}@C_{60}$  be isolated experimentally and become superconducting? *Nano Lett.* **17**, 3402–3408 (2017).
- Gromov, A., Kratschmer, W. & Campbell, E. Extraction and HPLC purification of  $\text{Li}@C_{60}/_{70}$ . *Chem. Commun.* **20**, 2003–2004 (1997).
- Aoyagi, S. et al. A layered ionic crystal of polar  $\text{Li}@C_{60}$  superatoms. *Nat. Chem.* **2**, 678–683 (2010).
- Gromov, A., Ostrovskii, D., Lassesson, A., Jönsson, M. & Campbell, E. E. B. Fourier transform infrared and Raman spectroscopic study of chromatographically isolated  $\text{Li}@C_{60}$  and  $\text{Li}@C_{70}$ . *J. Phys. Chem. B* **107**, 11290–11301 (2003).
- Ueno, H. et al. Electrochemical reduction of cationic  $\text{Li}^+@C_{60}$  to neutral  $\text{Li}^+@C_{60}^-$ : isolation and characterization of endohedral [60]fulleride. *Chem. Sci.* **7**, 5770–5774 (2016).
- Kubozono, Y. et al. Preparation and extraction of  $\text{Ca}@C_{60}$ . *Chem. Lett.* **24**, 457–458 (1995).

- Diener, M. D. & Alford, J. M. Isolation and properties of small-bandgap fullerenes. *Nature* **393**, 668–671 (1998).
- Ogawa, T., Sugai, T. & Shinohara, H. Isolation and characterization of  $\text{Er}@C_{60}$ . *J. Am. Chem. Soc.* **122**, 3538–3539 (2000).
- Inoue, T. et al. Electronic structure of  $\text{Eu}@C_{60}$  studies by XANES and UV-VIS absorption spectra. *Chem. Phys. Lett.* **316**, 381–386 (2000).
- Wang, Z. et al. Missing small-bandgap metallofullerenes: their isolation and electronic properties. *Angew. Chem. Int. Ed.* **52**, 11770–11774 (2013).
- Wang, Z., Aoyagi, S., Omachi, H., Kitaura, R. & Shinohara, H. Isolation and structural determination of a missing endohedral fullerene  $\text{La}@C_{70}$  through *in situ* trifluoromethylation. *Angew. Chem. Int. Ed.* **55**, 199–202 (2016).
- Hebard, A. F. et al. Superconductivity at 18 K in potassium-doped  $\text{C}_{60}$ . *Nature* **350**, 600–601 (1991).
- Ganin, A. Y. et al. Polymorphism control of superconductivity and magnetism in  $\text{Cs}_3\text{C}_{60}$  close to the Mott transition. *Nature* **466**, 221–225 (2010).
- Wang, C. R. et al.  $\text{C}_{66}$  Fullerene encaging a scandium dimer. *Nature* **408**, 426–427 (2000).
- Stevenson, S. et al. A stable non-classical metallofullerene family. *Nature* **408**, 427–428 (2000).
- Kareev, I. E. et al. Synthesis, structure, and  $^{19}\text{F}$  NMR spectra 1,3,7,10,14,17,23, 28,31,40-40- $\text{C}_{60}(\text{CF}_3)_{10}$ . *J. Am. Chem. Soc.* **127**, 8362–8375 (2005).
- Kuvychko, I. V. et al. In search of fullerene-based superacids: synthesis, X-ray structure, and DFT study of  $\text{C}_{60}(\text{C}_2\text{F}_5)_3\text{H}$ . *J. Am. Chem. Soc.* **127**, 8362–8375 (2005).
- Rayson, M. J. & Briddon, P. R. Rapid iterative method for electronic-structure eigen- problems using localised basis functions. *Comput. Phys. Commun.* **178**, 128–134 (2008).
- Rayson, M. J. & Briddon, P. R. Highly efficient method for Kohn-Sham density functional calculations of 500–10,000 atom systems. *Phys. Rev. B* **80**, 205104 (2009).
- Briddon, P. R. & Rayson, M. J. Accurate Kohn-Sham DFT with the speed of tight binding: current techniques and future directions in materials modelling. *Phys. Status Solidi B* **248**, 1309–1318 (2011).
- Hartwigsen, C., Goedecker, S. & Hutter, J. Relativistic separable dual-space Gaussian pseudopotentials from H to Rn. *Phys. Rev. B* **58**, 3641–3662 (1998).
- Funasaka, H., Sakurai, K., Oda, Y., Yamamoto, K. & Takahashi, T. Magnetic properties of  $\text{Gd}@C_{82}$  metallofullerenes. *Chem. Phys. Lett.* **232**, 273–277 (1995).
- Funasaka, H., Sugiyama, K., Yamamoto, K. & Takahashi, T. Magnetic properties of rare-earth metallofullerenes. *J. Phys. Chem.* **99**, 1826–1830 (1995).
- Huang, H., Yang, S. & Zhang, X. Magnetic properties of heavy rare-earth metallofullerenes  $\text{M}@C_{82}$  ( $\text{M} = \text{Gd}, \text{Tb}, \text{Dy}, \text{Ho}, \text{and Er}$ ). *J. Phys. Chem. B* **104**, 1473–1482 (2000).
- De Nadaï, C. et al. Local magnetism in rare-earth metals encapsulated in fullerenes. *Phys. Rev. B* **69**, 184421 (2004).
- Kitaura, R., Okimoto, H., Shinohara, H., Nakamura, T. & Osawa, H. Magnetism of the endohedral metallofullerenes  $\text{M}@C_{82}$  ( $\text{M} = \text{Gd}, \text{Dy}$ ) and the corresponding nanoscale peapods: synchrotron soft x-ray magnetic circular dichroism and density-functional theory calculations. *Phys. Rev. B* **76**, 172409 (2007).
- Sebetci, A. & Richter, M.  $\text{Gd}@C_{82}$ : origin of the antiferromagnetic coupling between endohedral Gd and the free spin on the carbon cage. *J. Phys. Chem. C* **114**, 15–19 (2010).
- Furukawa, K., Okubo, S., Kato, H., Shinohara, H. & Kato, T. High-field/high-frequency ESR study of  $\text{Gd}@C_{82}$ -I. *J. Phys. Chem. A* **107**, 10933–10937 (2003).
- Matsuoka, H. et al. Multifrequency EPR study of metallofullerenes:  $\text{Eu}@C_{82}$  and  $\text{Eu}@C_{74}$ . *J. Phys. Chem. B* **108**, 13972–13976 (2004).

## Acknowledgements

We thank David Tomanek for valuable discussion. The experimental part of this work was financially supported by MEXT/JSPS KAKENHI Grant Numbers JP16H06350 and JP16H02248. The SQUID measurement part was financially supported by the Private University strategic research infrastructure support program of MEXT based on green innovation research at Meiji University, S1511021. The theory part was financially supported by Region Pays de la Loire “Paris Scientifiques 2017” Grant Number 09375 and CCPL for computing resources. The synchrotron radiation experiments were performed at SPring-8 with the approval of the Japan Synchrotron Radiation Research Institute (JASRI) (Proposal No. 2017A1206 and 2017B1373).

## Author contributions

H.S. led the entire project and contributed to the experimental work, including synthetic apparatus design of the present metallofullerenes. A.N., M.N., H.N., K.I., and Z.W. contributed to the synthesis, purification, and crystal growth of the materials. H.O. and A.N. contributed to  $^{19}\text{F}$ -NMR measurement. K.F., T.Y., and T.K. contributed to the ESR measurement. S.B. contributed to the SQUID magnetic measurement. S.A. contributed to the synchrotron X-ray diffraction measurement at SPring-8 and the data analyses. J.R.

and C.E. contributed to the theoretical part of the work. H.S., T.K., S.B., S.A., H.O., and C.E. wrote the paper.

### Additional information

**Supplementary Information** accompanies this paper at <https://doi.org/10.1038/s41467-018-05496-8>.

**Competing interests:** The authors declare no competing interests.

**Reprints and permission** information is available online at <http://npg.nature.com/reprintsandpermissions/>

**Publisher's note:** Springer Nature remains neutral with regard to jurisdictional claims in published maps and institutional affiliations.



**Open Access** This article is licensed under a Creative Commons Attribution 4.0 International License, which permits use, sharing, adaptation, distribution and reproduction in any medium or format, as long as you give appropriate credit to the original author(s) and the source, provide a link to the Creative Commons license, and indicate if changes were made. The images or other third party material in this article are included in the article's Creative Commons license, unless indicated otherwise in a credit line to the material. If material is not included in the article's Creative Commons license and your intended use is not permitted by statutory regulation or exceeds the permitted use, you will need to obtain permission directly from the copyright holder. To view a copy of this license, visit <http://creativecommons.org/licenses/by/4.0/>.

© The Author(s) 2018